# Vision and force based autonomous coating with rollers

Yayun Du<sup>1</sup>, Zhaoxing Deng<sup>1</sup>, Zicheng Fang<sup>1</sup>, Yunbo Wang<sup>1</sup>, Taiki Nagata<sup>1</sup>, Karan Bansal<sup>2</sup>, Mohiuddin Quadir<sup>2</sup>, Mohammad Khalid Jawed<sup>1</sup>

Abstract—Coating rollers are widely popular in structural painting, in comparison with brushes and sprayers, due to thicker paint layer, better color consistency, and effortless customizability of holder frame and naps. In this paper, we introduce a cost-effective method to employ a general purpose robot (Sawyer, Rethink Robotics) for autonomous coating. To sense the position and the shape of the target object to be coated, the robot is combined with an RGB-Depth camera. The combined system autonomously recognizes the number of faces of the object as well as their position and surface normal. Unlike related work based on two-dimensional RGBbased image processing, all the analyses and algorithms here employ three-dimensional point cloud data (PCD). The object model learned from the PCD is then autonomously analyzed to achieve optimal motion planning to avoid collision between the robot arm and the object. To achieve human-level performance in terms of the quality of coating using the bare minimum ingredients, a combination of our own passive and builtin active impedance control is implemented. The former is realized by installing an ultrasonic sensor at the end-effector of robot working with a customized compliant mass-springdamper roller to keep a precise distance between the endeffector and surface to be coated, maintaining a fixed force. Altogether, the control approach mimics human painting as evidenced by experimental measurements on the thickness of the coating. Coating on two different polyhedral objects is also demonstrated to test the overall method.

## I. INTRODUCTION

Structural coating is labor-intensive and can be potentially detrimental to human health by irritating the skin and causing headaches, dizziness, and nausea. However, painting and maintenance needs are growing rapidly throughout the world, while the construction industry faces a potential shortage of skilled workers and increasing wages. Hence, robots are ideal alternatives to liberate manpower and improve productivity by concentrating on quality, safety, time, and cost savings. Paint spraying robots have been serving in specially equipped large workshops and buildings with precise CAD models of objects to be coated ready for multiple decades [1]. Due to the well-known drawbacks, prohibitive cost, and restricted applicability, airless methods of coating (e.g. roller-based) are significantly more popular in structural painting, e.g. painting the walls of a building.

With ever-improving maneuverability and flexibility, robots are also the perfect alternative to humans for the potentially hazardous task of coating objects in high risk situations [2]. This article lays the foundation for autonomous

coating by robots, as a replacement for painting by hand. Instead of building a new platform dedicated only to coating applications with limited reach access [3], [4], [5] or enabling robots to cooperate with humans to coat on general 2D flat surfaces [6], [7], we aim to utilize a dexterous robot – Sawyer (Rethink Robotics) – for coating on not only flat walls but also generic polyhedral objects and curved surfaces. Enabling a general purpose hardware to coat objects, instead of developing dedicated equipment that takes up additional space, is especially impactful for domestic robots.

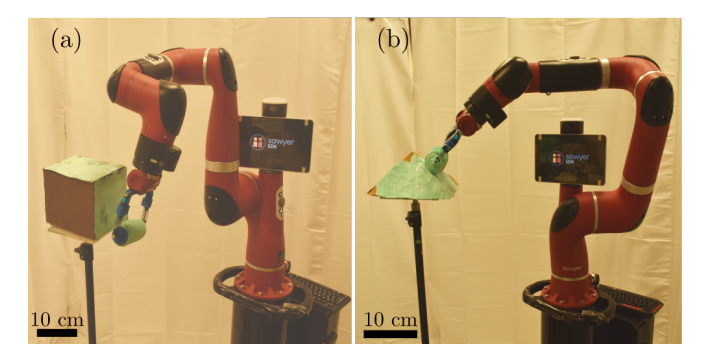


Fig. 1. Sawyer recognizes the object shape [(a) cuboid and (b) pyramid] and paints it using the three-dimensional point cloud data captured by the depth camera (not shown in the picture).

Here, we present the control framework to enable a robot to see, recognize, and coat the object (planar and curved surfaces) as well as avoid obstacles while moving its arm. Fig. 1 shows snapshots of the robot coating two different 3D objects. The roller trajectory on each surface of the target object is computed using three-dimensional point cloud data (PCD) from an RGB-Depth camera (Intel RealSense). The number, perimeters, and surface normals of planar faces of the object are computed through K-means clustering. To compensate the size and depth differences between the calculated and real target surfaces due to measurement error of the depth camera problem in a cost-effective way, a roller is designed that incorporates linear springs. In conjunction with an ultrasonic sensor attached to the end-effector of the robot, this compliant roller offers a passive impedance control that eventually allows us to maintain a constant force applied by the roller onto the surface. Although built-in impedance control in Sawyer is unable to perform uniform coating by itself, it can be useful in cases when the roller moves close to the edges of curved surfaces and the ultrasound fails to sense the distance to the surface. Two sets of experiments are conducted. First, autonomous coating on three-dimensional objects is performed that brings together quantification of

<sup>&</sup>lt;sup>1</sup>Department of Mechanical & Aerospace Engineering, University of California, Los Angeles, 420 Westwood Plaza, Los Angeles, CA 90095

<sup>&</sup>lt;sup>2</sup>Department of Coatings and Polymeric Materials, North Dakota State University, Fargo, 1340 Administration Ave, ND 58105

the target topology, motion planning, and collision avoidance between the robot arm and the object. Qualitative observation on coating performance on a cuboid and a pyramid indicates the possibility of using robots for autonomous coating in hazardous situations. Second, coating quality on a horizontal planar surface is compared against painting by hand. We find that the quality, quantified by coating thickness, attained by the robot using passive impedance control developed by us is comparable to painting by hand. It is also discovered that the combination of low-cost ultrasonic sensor and customized compliant roller is accurate enough to achieve painting with a constant force, thus ensuring coating uniformity.

In summary, our contributions are as follows: (1) A framework enabling a robot to recognize the shape of 3D objects, plan the coating trajectory autonomously and finally perform painting tasks with human-level quality is proposed. This framework is generally applicable to robots with only position control capability (not restricted to the specific collaborative robot used in this paper); (2) Bare minimum ingredients are used for the tasks, including the smart design of a compliant roller handle, functional while maintaining the system stability; (3) The same computationally efficient segmentation method is used for both trajectory planning and obstacle modeling with cubic spline interpolation to avoid jerky movements.

The paper is structured as follows: we review related work in Sec. II, followed by Sec. III in which we describe the theories and algorithms applied in our approach. Experiments and results are discussed in Sec. IV. Finally, Sec. V concludes the paper.

## II. RELATED WORK

Autonomous and adaptable robots for interior finishings are a very recent development with only a handful of prior works. TAMIR, a multi-purpose robot, was built for block laying and wall painting with multiple sprayers at the endeffector [6] but it mainly aims at human robot collaboration and cannot detect the location of the plane to be painted autonomously. A 3-DOF robot [8] was designed to automate upright spray painting for only ceilings by moving vertically via a zigzag ladder. However, its workspace is small in comparison with the platform size. A scaled down interior robot [9] was developed for laboratory research to study reproducing colored artworks utilizing a specially designed sprayer. Pictobot [7] aims at performing repetitious and tiresome painting at high elevations on tall walls. Less accurate but movable and more affordable platform [3] was developed but the painting quality is often not satisfactory. To compensate the shortcomings mentioned above and be more realistically adaptable to life, autonomous robots that possess automation and human-level skill are necessary. The overall cost and versatility of the system is another important factor. In the context of autonomous coating, robust integration of 3D shape recognition, hand eye cooperation, obstacle avoidance, and control modules are the main hurdles.

3D Shape Recognition is crucial for robots performing tasks autonomously in real world environments. Li-

DAR and RGB-Depth (RGB-D) cameras provide rich threedimensional data to assist different tasks and thus are increasingly popular in robotic systems. Compared with expensive LiDAR that mainly provides 3D mappings in exterior area [10], [11], cost-effective RGB-D cameras are more suitable for indoor object recognition and topology quantification [12]. Three-dimensional object recognition algorithms rely on local geometric features [13], corner detectors [14], and appearance recognition [15]. Despite the success of these methods, the computational cost motivates us to consider a simpler and computationally cheaper method for processing the PCD for our painting application.

Hand/eye calibration is significant in robotic manipulation owing to the need for transformation among different frames, e.g. the world frame and the moving frame attached to the end-effector [16]. Without hand/eye calibration, the robot cannot solely rely on the data from the vision sensors to determine how much 3D motion its joints have to undertake to move from one position to another desired location. This article employs a combination of depth camera and ultrasonic sensor for this purpose.

Autonomous path planning is an essential issue in any manipulation task for mobile robotic systems. The goal of path planning is to find a non-collision continuous path for a robotic manipulator from the initial to the end pose in a configuration space with the manipulator's constraints satisfied. For robotic coating, this also requires avoiding the target objects. The most popular motion planning algorithms used to avoid obstacles include OMPL [17], CHOMP [18] and convex optimization method [19]. In this study, OMPL real-time motion planner in MoveIt! [20], a freely and publicly available motion planning software, was employed.

#### III. THEORIES AND ALGORITHMS

### A. 3D shape recognition

The coating task begins with the recognition of the shape of the target object. The object is originally treated as a polyhedron enclosed by a finite number of planar faces. As detailed next in this section, the raw RGB-D information of the object generated from the depth camera is used to extract the geometric features through surface normal estimation and machine learning algorithms. The ultimate goal is to identify the number of faces visible in the PCD and the associated surface normals. In the experiment setup, the camera is fixed at a location on the ground from where the object to be painted can be seen. Two example objects are used: (i) a cuboid of size  $16\text{cm} \times 13\text{cm} \times 13\text{cm}$ , and (ii) a quadrangular pyramid whose side surfaces are isosceles triangles with 13cm hypotenuse and base is a square with 16cm side length. The RGB-D data of the object are processed using the following steps. Fig. 2 outlines these steps for the case of a cuboid.

1) Downsampling & Outlier Removal: The large amount of PCD can be unnecessarily computationally expensive. To reduce the number of points, we downsample them to a voxel of size 0.001 m. Due to variations in point densities in the point cloud and measurement error of the depth camera,

the sparse outliers may lead to errors in normal estimation. These outliers are removed using simple statistical analysis that examines the relative distance among the points. The ones that are far from all the other points are deleted from the PCD. Fig. 2(a) shows the data after downsampling and outlier removal.

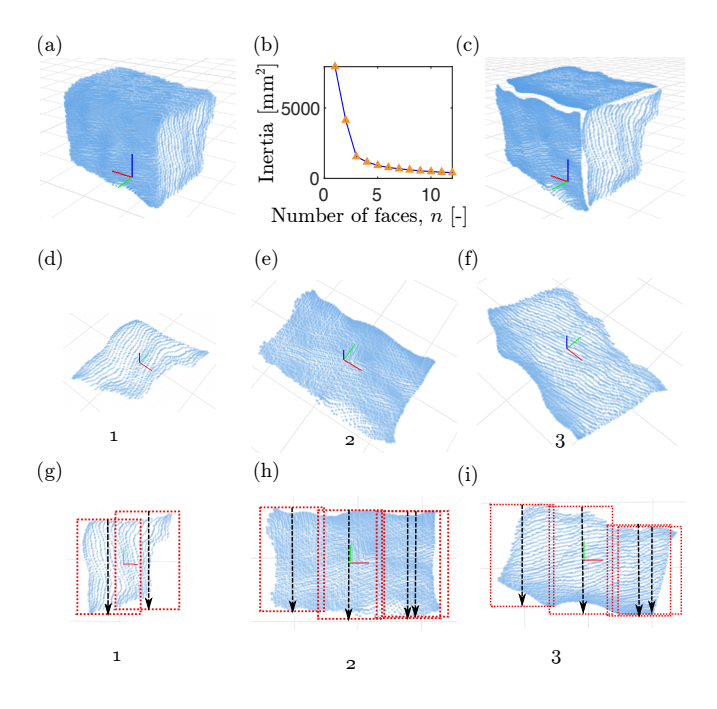


Fig. 2. PCD processing. (a) Background and outliers-removed, smoothed PCD from the original PCD. (b) K-Means 'Elbow' method applied to the PCD in (a); three planes are identified. (c) Reconstructed object after fitting the planes and projecting the points to corresponding planes. (d)-(f) Separation of PCD into three planes and the local frame on each plane. (g)-(i) Motion of the roller on each surface. The red rectangles, with width equal to the width of the roller, represent each stroke.

- 2) Moving Least Square (MLS): Due to the slight inaccuracy of distance measurement by the depth camera and invalid depth data for some points, the downsampled PCD can still contain irregularities. One solution is to employ the MLS algorithm to resample the data, which uses polynomial interpolations between nearby data points to recreate the surface. This way, the data will be smoothed and estimation of the surface normal can be improved. In our implementation, we set the polynomial order to 2 and the search radius to  $r=1.5\,$  mm.
- 3) Estimating Surface Normal: At this stage, the PCD can be used to compute the normal direction at each point. These directions will be later analyzed to identify the number of unique normals; this is equal to the number of faces that need to be coated. The solution to estimating the surface normal is reduced to the analysis of eigenvectors and eigenvalues of a covariance matrix created from the nearest neighbors of each point. The covariance matrix is

$$\mathbf{C} = \frac{1}{k} \sum_{i=1}^{k} \cdot (\mathbf{p}_i - \bar{\mathbf{p}}) \cdot (\mathbf{p}_i - \bar{\mathbf{p}})^{\mathsf{T}}$$
(1)

where k is the number of points considered as neighbors of point  $\mathbf{p}_i$  and  $\bar{\mathbf{p}}$  is the centroid of point neighbors. We set k to 30; this value is estimated based on the density of the PCD and the approximate size of the target object.

4) K-Means Clustering: The K-Means clustering algorithm is used to automatically learn the number of object surfaces by clustering the normal at each point into several groups. The number of groups is essentially equal to the number of faces, n, of the object. The corresponding optimization problem can be stated as follows: divide N points into n clusters that minimize

$$SSE = \frac{1}{N} \sum_{i=1}^{N} ||\mathbf{x}_i - \mathbf{z}_{c_i}||^2,$$
 (2)

where  $\mathbf{x}_i$  represents the position of each point and  $\mathbf{z}_{c_i}$  denotes the center of the i-th group. Since K-Means clustering needs the cluster number n as an input, which varies n from 1 to a large integer, calculate the sum of squared errors (SSE) for each n, and find the elbow with the lowest SSE. The line chart of the elbow method for a cuboid box is presented in Fig. 2(b). Note that there is a dramatic drop of SSE (i.e. inertia) at n=3 and, as a result, the robot decides that the object has 3 surfaces exposed to the camera. While our method can handle objects with a priori unknown number of planar surfaces, it has to collaborate with passive impedance control talked later in III-D to paint curved surfaces.

## B. Projective Plane Fitting & Trajectory Planning

With PCD that have been divided into n clusters, the next step is to find the best plane to fit each cluster of points by minimizing the sum of square distance from each point to the constructed plane.

Referring to Fig. 3, our system consists of a camera, the robot, and the target object. We treat the camera as the robot's eye and the end-effector as its hand. The object information is obtained once the eye captures it under the camera frame  $\{C\}$ ; the data is then transformed to the robot's base frame  $\{W\}$ , i.e. the world frame. After the surface normals are computed from the PCD, the points are grouped into multiple planes. A local frame  $\{L\}$  for each plane is

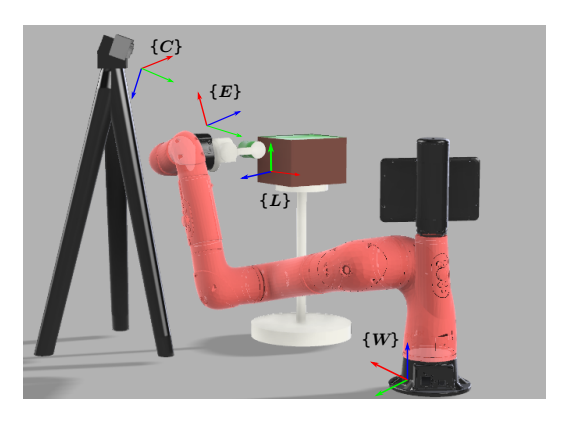


Fig. 3. Different frames in the experiment setup.  $\{C\}$  is the camera frame,  $\{E\}$  is the robot end-effector frame,  $\{L\}$  denotes the local frame on each object surface, and  $\{W\}$  stands for the robot-base frame or world frame.

constructed; the planes are denoted as 1, 2, and 3 in Fig. 2(c). The z-axis of the local frame is parallel to the surface normal, whereas the x- and y-axes lie on the plane.

With local frames defined, let's move to roller trajectory planning. The z-axis of the end-effector frame,  $\{E\}$ , is oriented along the normal to the plane to be coated, i.e. z-axis of  $\{L\}$ . The end-effector, with the attached roller, moves along the y-axis of the local frame,  $\{L\}$ . Red dashed rectangles with width equal to the roller width in Fig. 2 (g)-(i) represent the traces of the roller. The length of each rectangle (along the y-axis of  $\{L\}$ ) is computed based on the maximum and minimum x-coordinate (in  $\{L\}$  frame) of the points of the PCD that fall in that rectangle. During the stroke planning of the roller, an overlap between the two adjacent rectangles and the extended length at the beginning of each stroke, based on the extracted shape of each surface from the point cloud, are set as adjustable parameters to ensure the coating completeness.

#### C. Motion Planning & Obstacle Avoidance

With the 3D data processed, the robot knows the number of surface to be coated as well as the position and orientation of each surface. For collision avoidance between the robot and environment when the robot end-effector moves on each face and from one face to another, OMPL [17] real-time motion planner is used. As shown in Figs. 2(g)-(i), each plane is segmented into rectangles treated as both coating path and obstacles as a whole. The waypoints are generated through cubic spline interpolation between the upper and lower sides of the dashed rectangles with position, velocity, and acceleration calculated. The dashed arrows denote the moving direction of the roller and orientation of the end-effector is set to align z-axis of  $\{E\}$  frame with z-axis of  $\{L\}$  frame in Fig. 3.

Obstacle avoidance is realized simultaneously with the trajectory planning problem through the same computationally efficient segmentation method as shown in Fig. 2(g)-(i) and explained in Section III-B.

### D. Passive Impedance Control

Hand painting applies force and position control in a hierarchical but cooperative way. Position control moves the roller near the wall first and then force control comes into play to ensure an even painting. There are two main approaches for position-force control of manipulators: impedance control [21] and hybrid position-force control [22]. In impedance control, the impedance between the robot and environment is programmable and force can be fed back when position is controlled. Hybrid position-force control enables each degree of freedom to be controlled under a single modality, either position or force. When the manipulator of Sawyer is commanded to follow a prescribed trajectory in Cartesian space, the dynamic model of degrees of freedom can be expressed as

$$\mathbf{M}(\ddot{\mathbf{q}} - \ddot{\mathbf{q}_d}) + \mathbf{K}(\mathbf{q} - \mathbf{q}_d) + \mathbf{D}(\dot{\mathbf{q}} - \dot{\mathbf{q}_d}) = \mathbf{F}_{\text{ext}}$$
 (3)

where  $\mathbf{q}$  and  $\mathbf{q}_d$  denote the actual and desired joint displacement respectively, () represents derivative with respect to time,  $\mathbf{M}$  is the positive-definite diagonal inertia matrix, and  $\mathbf{K}$  and  $\mathbf{D}$  are diagonal matrices containing the robotic system control parameters related to spring stiffness and damping coefficient in each joint respectively.  $\mathbf{F}_{\text{ext}}$  includes all the external forces from the environment, primarily composed of the reaction force from the target surface along the direction of the surface normal. Note that we do not solve Eq. 3 explicitly, but rather the robot's software uses this type of model to implement active impedance control.



Fig. 4. End-effector (compliant roller) comprised of (1) A microcontoller and an ultrasonic sensor, (2) spring-damper system, and (3) roller cover.

The maximum spring stiffness at each joint is provided by the merchant, so matrix K in Eq. 3 can be controlled according to different tasks and orientations while D is not controllable by users. Due to the fact that no direct force/torque sensors are necessary for impedance control [23], the accuracy of force control is limited; this will be shown later using Fig. 7. In contrast, the accuracy of position control in industrial robots is millimeter-scale. Thus, there are two solutions to realize accurate force control in painting, either attach a costly force sensor or control force by position control ingeniously. Apparently, the latter is a better choice considering the cost and the erosion of force sensor if installed inside or near the roller. Hence, we design a cheap but practical compliant roller - a roller cover is attached to a spring system (based on BOLZR 108004 Aluminum Shock Absorber) which in turn is attached to the robot arm. The 3D-printed light-weight roller handle is equipped with a not overly flexible spring and a guide restricting the compliance of the roller only along the z-direction, the most sensitive direction of force sensor inside the tool plate. For the stability of the system, the speed of movement along the z-direction during painting is prevented from being large. The end-effector model, the roller, is also updated in the Unified Robot Description Format (urdf) format that is imported when planning is carried out. In summary, the system stability, minimization of decrease of force detection sensitivity and modeling accuracy are all considered in our design. Fig. 4 shows different components of the compliant roller.

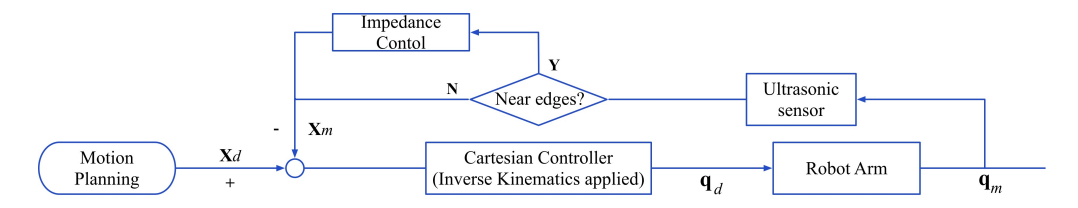


Fig. 5. Our overall control approach. Here,  $\mathbf{X}_d$  and  $\mathbf{X}_m$  are the desired endpoint position of the robot and the one measured by the ultrasonic sensor, respectively.  $\mathbf{q}_d$  and  $\mathbf{q}_m$  are the vector containing desired and actual seven joint positions of the robot, respectively.

In the context of coating, once the robot touches the object surface and tries to get to the desired position, the spring of the compliant roller is compressed resulting in the external force,  $\mathbf{F}_{\text{ext}}$ . The force can be approximated to be kx, where k is the spring stiffness and x is the compressed distance. Maintaining a constant x in the normal direction of target surface ensures constant force during each stroke. Using an ultrasonic sensor (LGDehome HC-SR04) attached to the robot arm (see Fig. 4), combined with a microcontroller (Adafruit Pro Trinket 5V), the distance between the endeffector and target surface can be published through ROS messages and continuously monitored by the robotic arm. Essentially, our method has two typical characteristics of impedance control: compliance and target point accomplishment through position control but fails in programmable stiffness. Therefore, we call it passive impedance control.

The overall control approach is shown in Fig. 5. In autonomous 3D object coating, due to errors in depth measurement and uncertainties associated with fitting, vision alone is not reliable. Therefore, our reconstructed surfaces from the vision data may not exactly coincide with the real physical surfaces. Our first attempt at coating using pure position control and rigid off-the-shelf roller suggested that these inaccuracies must be corrected for successful coating. With its trajectory planned, i.e.  $X_d$  is known, when the robotic arm is far from the surfaces to be coated, the robot is purely controlled by position control and it moves its joints to the positions calculated by the Cartesian controller. When the roller handle aligns with the normal direction of the target surface, our proposed passive impedance control is activated. The robot moves until the roller touches the plane and begins coating under supervision of the ultrasonic sensor. In some cases, during the last stroke (near the edges of the surface), it is likely that ultrasound is reflected by other surfaces rather than the target surface. In this case, passive impedance control is stopped and the built-in impedance control of the robot is started to complete coating. Our passive impedance control is indirectly related to position control with gravity compensation and the addition of the compliant roller varies the overall stiffness matrix in Eq. 3 a little bit but can be compensated by the programmable stiffness values in built-in impedance controller so the closed-loop is still stable. While we did not encounter any issues with the stability of the closed loop system, it should be kept in mind during the design of the system. Experiment results will be given in Section IV-B.

This technique of utilizing a low-cost ultrasonic sensor,

with a compliant roller for force control is another key contribution of this paper. While robots feature precise position control, they are not equipped with accurate enough force and torque sensors. Even though it is possible to equip a robot with force sensors of desired precision and accuracy, this solution can be cost prohibitive and hard to implement. Our proposed method, on the other hand, is cheap and, as discussed in the next section, achieves reasonable coating quality.

#### IV. EXPERIMENTS & RESULTS

Autonomous coating by the collaborative robot, following the above framework, is carried out on two types of objects: (i) 3D polyhedral objects (a cuboid and a pyramid) and (ii) 2D horizontal and planar surface.

#### A. 3D Cuboid and Pyramid Boxes

With autonomous coating in hazardous environments in mind, we test the ability of our framework to quantify the topology of unknown objects and coat their surfaces. Two different objects are used: a cuboid and a pyramid (physical dimensions are provided in Sec. III). The robot can successfully detect the faces facing the camera and coat with more than 90% completeness. It cannot achieve a perfect coating due to unevenness of the roller surface and physical limitations imposed by the workspace of the robot. The roller sometimes may get stuck at corners of the objects so the robot will avoid them, leaving uncoated corners. Apart from the object shape and size recognition, path planning and obstacle avoidance functions, the quality evaluation of 3D painting is nothing different from 2D painting. Also, in addition to coating in hazardous environment, 3D wall and ceiling painting – our target area of application – simply includes smooth movement on 2D planar surfaces and switching from one to the other perpendicular plane. Therefore, we will put emphasis on the 2D coating evaluation.

# B. 2D Horizontal Planar Surface

Quality of the paint, coating evenness and thickness are three main factors that decide the painting performance. We choose Behr's most advanced ceiling paint (Behr Marquee Fish Pond P440-3) to ensure the paint quality. Coating evenness and thickness, on the other hand, are geometric properties that can be controlled by the painter. Motivated by potential application in painting walls and ceilings, we test the quality of coating on 2D planar surfaces. The surface is formed by assembling multiple aluminum panels  $(3 \times 6 \text{ in}^2)$ 

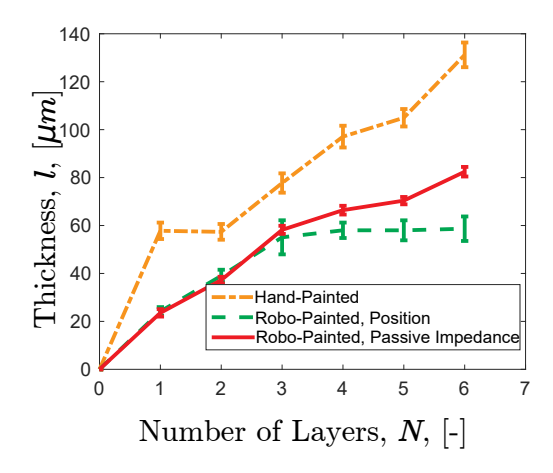


Fig. 6. Coating thickness comparison between human and robot

side-by-side on a rigid base. After coating with ceiling paint, the panels are removed from the base for measurement of the coating thickness, l. Fig. 6 shows the thickness measured by a digital meter (ERAY Coating Thickness Gauge), l, as a function of the number of layers, N (i.e. number of strokes on each point of the surface) for three different cases: (i) coating by hand (rigid roller; Wooster Super Doo-Z  $4in \times 3/8in$ ), (ii) robotic coating with only position control (rigid roller), and (iii) robotic coating with passive impedance control (compliant roller and ultrasonic sensor) to realize an 8N constant force. A key metric for evaluation of the coating quality is the linear relationship between the thickness and the number of layers. In case of coating by hand and robotic coating with force-position control, the data points can be fitted by a line to a good approximation. In fact, robotic coating seems to provide a better fit than coating by hand. The slope of the line can vary with a number of factors, e.g. applied force, and, as a result, we are not concerned with matching the numerical value of this slope between hand coating and robotic coating. On the other end, coating with only position control does not result in a linear relationship between thickness and the number of layers. The thickness reaches approximately  $60 \mu m$  and does not show significant variation with the number of layers beyond N=3. The reason can be explained through Fig. 7(a) that shows the data for one experimental trial. In most orientations, even if an 8N force is initially applied onto the roller under pure position control mode, the robot arm might drift away from the surface or press the roller too hard at the next moment. In Fig. 7(a), point A is the time when robotic arm drifts and barely touches the surface, so the painting thickness is not increasing anymore. If the roller is pressed too hard, the thickness also does not vary significantly with the number of layers. This emphasizes the need for passive impedance control using the ultrasonic sensor during robotic coating.

The other key metric for determining the coating quality is consistency, namely the ability to maintain a constant force while painting. Before starting the experiments, we build the map from distance between the ultrasonic sensor and surface, d, to force applied onto the surface, F, by the customized compliant roller. As expected from linear spring model, the relation between F and d is approximately linear. For example, if an 8N force, measured by a push pull force gauge (Beslands NK-500), is expected to be applied, the distance should be kept at  $13.75\,\mathrm{cm}$ , called the distance threshold denoted by the dashed blue line in Figs. 7(b). Sawyer continuously checks the distance and keeps it at the threshold. The distance variation when robot paints with a constant force using passive impedance control is within  $4\,\mathrm{mm}$ , 3% error in force.

Then we program the impedance of each joint and apply a force limit 8N with impedance control, using the robot's proprietary software and the force read by the robot is shown in Fig. 7(c). It is clear that impedance control is unable to control a specific force because of the lack of force sensors as mentioned in Section III-D. However, it is helpful to confirm that the edges are also painted in cases where the ultrasonic sensor fails due to missing ultrasound echoes reflected back near surface edges. In addition, the quality and force evaluation was performed using 2D surfaces held rigidly in place. In the case of coating 3D cuboid and pyramid boxes in our experimental setup, the target surface would slightly shake upon contact with the roller and force evaluation in this case would be unreliable.

In summary, our framework, the combination of a depth camera with a robotic arm with position control capability, enables online recognition of the 3D object shape, trajectory planning and painting realization. In addition, our economical method using the ultrasonic sensor together with the customized compliant roller accomplishes coating of high quality as shown in both Fig. 6 and Fig. 7(b), where built-in impedance control fails. In the future, other parameters for quality measurement (e.g. hardness, impact resistance, color, etc.) in addition to thickness should be quantified for robotic coating.

# V. CONCLUSIONS AND FUTURE DIRECTIONS

We introduced a comprehensive framework for autonomous coating using a collaborative robot and threedimensional PCD acquired by a depth camera. This method unites hand-eye cooperation, geometry processing, obstacle avoidance, and the incorporation of passive impedance control developed by us and the built-in impedance control in the robot. Specifically, the control approach combines position control with feedback from a low-cost ultrasound sensor and a spring-like compliant roller handle and impedance control. Just like humans, the robot can maintain a constant force between the roller and the target surface. The quality of coating by the robot is compared against coating by hand. The results show the effectiveness of the control algorithm in achieving human-level performance. Further experiments using polyhedral objects demonstrate the ability of the framework to quantify the topology of the object and coat on its faces. We hope that this study will potentially enable application of collaborative robots for coating applications in the household or hazardous environments.

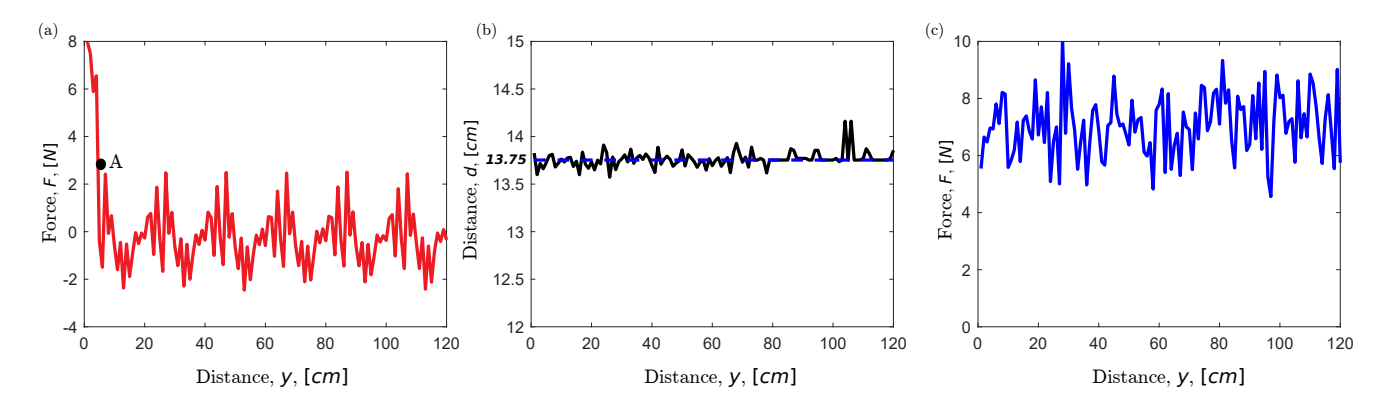


Fig. 7. Force as a function of the distance robot end-effector/roller moves of different control regimes to keep a 8N force when robotic arm paints. (a) No force control. (b) Passive impedance control with an ultrasonic sensor attached at the end-effector. (c) Built-in impedance control. Here, y is the coordinate along the length of the target surface.

We envision three directions for future work. First, our current work is limited to coating a subset of the faces of a small object. In order to coat larger surfaces, the robot can be made mobile horizontally and vertically by adding actuators to the wheeled pedestal. Instead of a single depth camera, multiple cameras can be fused to quantify all the faces of the object. Manipulation of the target object by the robot to coat all the faces can also be considered. Second, the proposed framework can handle a finite number of planar surfaces and simple curved surfaces; curved surfaces with continuously varying surface normal, e.g. a sphere, were not considered. We hope that the proposed framework lays the foundation for future work on coating complex non-planar surfaces. Third, operation planning of the robot, incorporating vision, motion planning, obstacle avoidance, and feedback (coating quality), can be investigated.

### ACKNOWLEDGMENTS

We acknowledge support from the National Science Foundation (Award # IIS - 1925360) and the Henry Samueli School of Engineering and Applied Science, University of California, Los Angeles.

#### REFERENCES

- [1] A. Vecellio, "Robot painting system for automobiles," U.S. Patent 4,532,148, 1983.
- Y. Baudoin and M. K. Habib, Using robots in hazardous environments:
   Landmine detection, de-mining and other applications. Elsevier, 2010.
- [3] H. Kim, D. Ko, B. Jung, M. Lee, and S. Lee, "Large size painting with infraless vision-aided mobile robot," in 2018 18th International Conference on Control, Automation and Systems (ICCAS), pp. 325–330, IEEE, 2018.
- [4] M. T. Sorour, M. A. Abdellatif, A. A. Ramadan, and A. A. Abo-Ismail, "Development of roller-based interior wall painting robot," <u>World Academy of Science, Engineering and Technology</u>, vol. 59, 2011
- [5] M. Abdellatif, "Design of an autonomous wall painting robot," Mechatronics and Robotics Dept. Egypt-Japan University of Science and Technology, Alexandria, Egypt, 2012.
- [6] B. Kahane and Y. Rosenfeld, "Balancing human-and-robot integration in building tasks," <u>Computer-Aided Civil and Infrastructure</u> <u>Engineering</u>, vol. 19, no. 6, pp. 393–410, 2004.
- [7] E. Asadi, B. Li, and I.-M. Chen, "Pictobot: a cooperative painting robot for interior finishing of industrial developments," <u>IEEE Robotics</u> & Automation Magazine, vol. 25, no. 2, pp. 82–94, 2018.

- [8] I. Aris, M. P. I. AK, A. Ramli, and S. Shamsuddin, "Design and development of a programmable painting robot for houses and buildings," Jurnal Teknologi, vol. 42, no. 1, pp. 27–48, 2005.
- [9] B. Naticchia, A. Giretti, and A. Carbonari, "Set up of an automated multi-colour system for interior wall painting," <u>International Journal</u> of Advanced Robotic Systems, vol. 4, no. 4, p. 50, 2007.
- [10] A. B. Davies and G. P. Asner, "Advances in animal ecology from 3d-lidar ecosystem mapping," <u>Trends in ecology & evolution</u>, vol. 29, no. 12, pp. 681–691, 2014.
- [11] A. Antonarakis, K. S. Richards, and J. Brasington, "Object-based land cover classification using airborne lidar," <u>Remote Sensing of environment</u>, vol. 112, no. 6, pp. 2988–2998, 2008.
- [12] K. Lai, L. Bo, X. Ren, and D. Fox, "A large-scale hierarchical multiview rgb-d object dataset," in 2011 IEEE international conference on robotics and automation, pp. 1817–1824, IEEE, 2011.
- [13] D. G. Lowe et al., "Object recognition from local scale-invariant features.," in iccv, vol. 99, pp. 1150–1157, 1999.
- [14] Z. Zhang, R. Deriche, O. Faugeras, and Q.-T. Luong, "A robust technique for matching two uncalibrated images through the recovery of the unknown epipolar geometry," <u>Artificial intelligence</u>, vol. 78, no. 1-2, pp. 87–119, 1995.
- [15] H. Murase and S. K. Nayar, "Visual learning and recognition of 3d objects from appearance," <u>International journal of computer vision</u>, vol. 14, no. 1, pp. 5–24, 1995.
- [16] R. Y. Tsai and R. K. Lenz, "A new technique for fully autonomous and efficient 3d robotics hand/eye calibration," <u>IEEE Transactions on robotics and automation</u>, vol. 5, no. 3, pp. 345–358, 1989.
  [17] I. A. Sucan, M. Moll, and L. E. Kavraki, "The open motion planning
- [17] I. A. Sucan, M. Moll, and L. E. Kavraki, "The open motion planning library," <u>IEEE Robotics & Automation Magazine</u>, vol. 19, no. 4, pp. 72–82, 2012.
- [18] M. Zucker, N. Ratliff, A. D. Dragan, M. Pivtoraiko, M. Klingensmith, C. M. Dellin, J. A. Bagnell, and S. S. Srinivasa, "Chomp: Covariant hamiltonian optimization for motion planning," <u>The International</u> Journal of Robotics Research, vol. 32, no. 9-10, pp. 1164–1193, 2013.
- [19] J. Schulman, J. Ho, A. X. Lee, I. Awwal, H. Bradlow, and P. Abbeel, "Finding locally optimal, collision-free trajectories with sequential convex optimization.," in <u>Robotics: science and systems</u>, vol. 9, pp. 1– 10, Citeseer, 2013.
- [20] S. Chitta, "Moveit!: an introduction," in <u>Robot Operating System</u> (<u>ROS</u>), pp. 3–27, Springer, 2016.
- [21] N. Hogan, "Impedance control of industrial robots," <u>Robotics and Computer-Integrated Manufacturing</u>, vol. 1, no. 1, pp. 97–113, 1984.
- [22] M. H. Raibert and J. J. Craig, "Hybrid position/force control of manipulators," 1981.
- [23] S. Tachi, T. Sakaki, H. Arai, S. Nishizawa, and J. F. Pelaez-Polo, "Impedance control of a direct-drive manipulator without using force sensors," Advanced Robotics, vol. 5, no. 2, pp. 183–205, 1990.